Optical bistability in a two-section InAs quantum-dot laser

Jiang Liwen(姜立稳)†, Ye Xiaoling(叶小玲) , Zhou Xiaolong(周晓龙), Jin Peng(金鹏), Lü Xueqin(吕雪芹), and Wang Zhanguo(王占国)

(Key Laboratory of Semiconductor Materials Science, Institute of Semiconductors, Chinese Academy of Sciences, Beijing 100083, China)

Abstract: Room temperature, continuous-wave bistable operation is achieved in two-section 1.24 μm InAs quantum-dot (QD) lasers with integrated intracavity QD saturable absorbers (SA). It is found that the hysteresis width is narrowed with increasing reverse bias voltage, and broadened with increasing length of saturable absorber. This can be explained by the competition between QD absorption and electroabsorption in the SA section. In addition, a larger hysteresis width is realized than other reports so far, which can be attributed to a greater number of stacked layers of active region in our case. The experimental results can be explained by a modified threshold current model.

Key words: absorption saturation; optical bistability; quantum-dot lasers; saturable absorber
DOI: 10.1088/1674-4926/31/11/114012 **PACC:** 4255P; 6322

1. Introduction

Self-assembled quantum dots (QDs) have potential as saturable absorbers (SAs), since they exhibit nonlinear saturable absorption properties[1] and ultrafast carrier dynamics[2]. With a QD SA integrated into a Fabry–Perot cavity, the two-section QD laser has shown unique characteristics, such as optical bistability[3, 4], self-pulsations and mode-locking[5, 6]. In particular, optical bistablity may lead to important applications in optical transmitters, memory elements and photonic switching. However, until now, only a few groups have observed the power bistability in two-section QD lasers, which have different device configurations and active regions[2, 3, 7, 8]. So far as we know, the hysteresis width, which is an important parameter for bistable operation, is no more than 50 mA. In addition, the effects of QD SA on the output light power–current (L–I) characteristics have not been fully investigated.

Here, we increase the number of stacked QD layers in the SA section to improve the bistability and study the L–I characteristics of two-section QD lasers experimentally. All the laser diodes were tested at room temperature and exhibited prominent optical bistability with the SA under appropriate bias conditions. The effects of bias conditions and SA length on the characteristic of bistability are investigated in detail. The competition effects of both QD absorption and electroabsorption are discussed based on a proposed threshold current model.

2. Device structure and fabrication

The QD laser investigated was grown on an n^+-GaAs substrate using our Riber-32 molecular beam epitaxy (MBE) system. The active region, which consists of an eleven fold stack of InAs QDs separated by 35 nm GaAs spacer layers, was situated in the middle of a 120 nm thick GaAs waveguide embedded in 2.2 μm AlGaAs cladding layers with graded refractive index. The 21.3 μm wide ridge waveguide laser structure was fabricated using a standard photolithography and wet etch process. The devices have a typical two-section laser structure with a 32.5 μm gap in the top p-type contact metals. A simplified schematic of laser structure is illustrated in Fig. 1. Three samples with different cavity configurations were fabricated, named S303, S306 and S309. The lengths of the gain section and the SA section of the three samples are L_g = 3 mm and L_a = 0.3 mm (S303); L_g = 3 mm and L_a = 0.6 mm (S306); L_g = 3 mm and L_a = 0.9 mm (S309), respectively. The isolation resistances are 0.549, 0.572 and 0.576 kΩ, respectively. The devices were mounted on a copper heat sink with the p-side up, and they were tested under continuous-wave (CW) lasing operation at room temperature.

3. Results and discussion

The devices were measured with current injection into the gain section (I_g) and the SA section under different bias conditions. Room-temperature CW lasing occurred on the QD

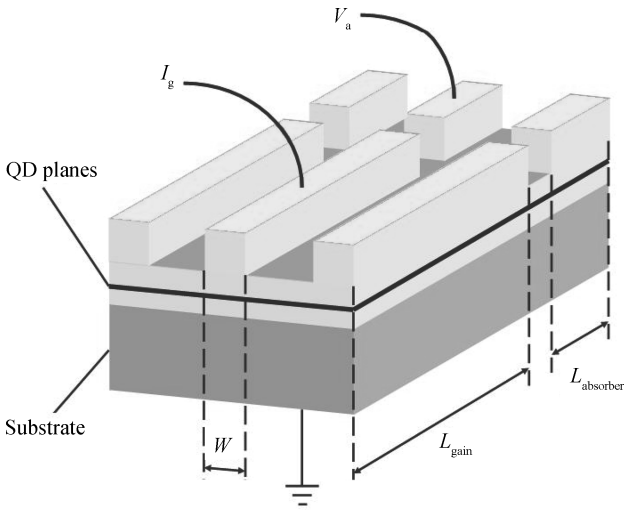

Fig. 1. A simplified schematic of the two-section QD laser. W: ridge width; I_g: forward current; V_a: reverse bias voltage; L_{gain}: length of gain section; $L_{absorber}$: length of SA section.

† Corresponding author. Email: tonyjiang1124@semi.ac.cn
Received 30 April 2010

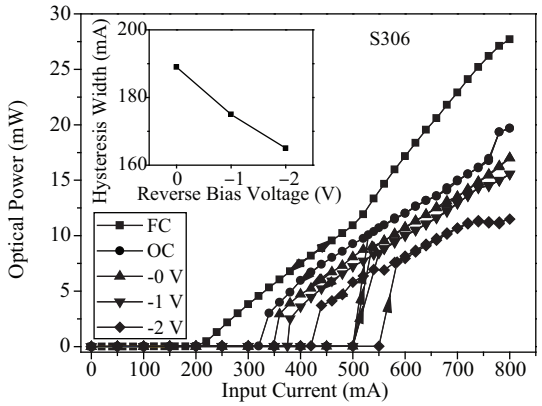

Fig. 2. Light-current characteristics of the 3.6-mm-long device with a 600-μm-long absorber section for different reverse bias voltages. The inset shows the hysteresis width of S306 versus the reverse bias voltage.

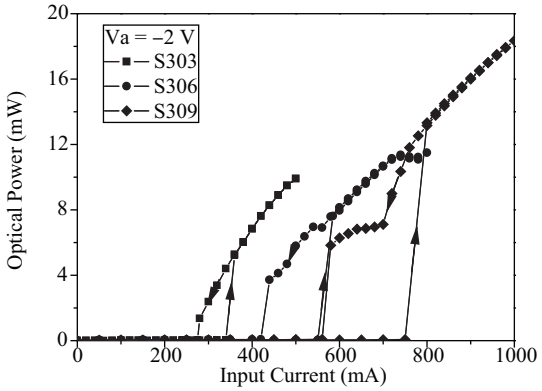

Fig. 3. Light-current characteristics of devices with different configurations under reverse bias voltages of 2 V.

ground state at a center wavelength of 1.24 μm. Figure 2 shows the output light power of S306 emitting from the absorber facet versus the forward and backward sweep of the laser current under five different absorber bias conditions. The L–I characteristics exhibit clear counterclockwise hysteresis loops and bistability when the SA section is applied with a constant reverse bias voltage (V_a) or under the condition of open circuit (OC). With increased V_a, the loop position shifts to a higher laser current, while the output power of the laser diode is decreased at the same current. Additionally, when the two sections are under a fully connected (FC) situation, the lasers behave as normal lasers and no hysteresis loop is observed. The inset of Fig. 2 shows that the hysteresis width of S306 also decreases with increased V_a, which will be discussed later.

The effects of the length of the SA section on the L–I characteristics are shown in Fig. 3, with 2 V constant reverse voltage applied to the SA section. Both threshold current and hysteresis width are increased for a longer SA section. The hysteresis loop width of S309 reaches 240 mA, and the on-off ratio is 129 : 1 at the center of the hysteresis loop, which are far beyond the results of Refs. [3, 4, 7, 8].

A modified model of threshold current is used to analyze the effects of reverse bias voltage and length of the SA section on threshold current and hysteresis width. Figure 4 shows the schematic of propagation of light along the z axis in the

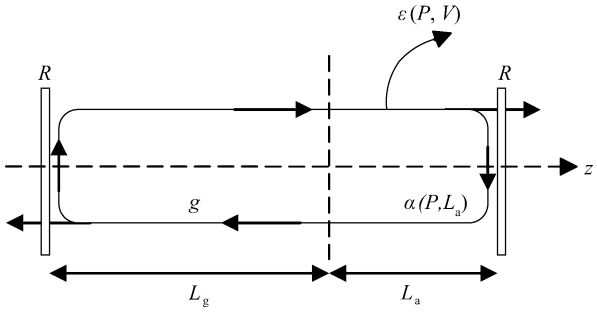

Fig. 4. Schematic of the propagation of light along the z axis in the resonant of a two-section laser.

resonator, where g is the net gain coefficient in the gain section. We define α and ε as the loss coefficient of QD absorption and electroabsorption in the SA section, respectively, both of which are related to the output light power P. From the definition, it can be imagined that α and ε are related to the total density of QD states and the reverse voltage in the SA section, respectively. L_g and L_a are the length of the gain section and the SA section, respectively. R is the reflectivity of both facets of the laser. The increment of light intensity with propagating a dz distance in the gain section is

$$\mathrm{d}I(z) = gI(z)\mathrm{d}z, \tag{1}$$

in which $I(z)$ is the light intensity at position z.

Equation (1) can be written as

$$\frac{\mathrm{d}I(z)}{I(z)} = g\mathrm{d}z. \tag{2}$$

The integration form of Eq. (2) is

$$\int_{I(0)}^{I(z)} \frac{\mathrm{d}I(z)}{I(z)} = \int_0^z g\mathrm{d}z, \tag{3}$$

$$I(z) = I(0)\exp(gz), \tag{4}$$

where $I(0)$ is the initial light intensity at position $z = 0$.

Similarly, $I(z)$ in the SA section is given by

$$I(z) = I(0)\exp[-(\alpha+\varepsilon)z]. \tag{5}$$

When the light circulates in the cavity once and finally back to the position $z = 0$, the light intensity can be deduced as

$$I(z) = R^2 I(0)\exp[2gL_g - 2(\alpha+\varepsilon)L_a]. \tag{6}$$

If $I(z)$ is equal to $I(0)$, the equation represents the threshold condition of the laser, which can be written as

$$g = (\alpha+\varepsilon)\frac{L_a}{L_g} + \frac{1}{2L_g}\ln\frac{1}{R^2}. \tag{7}$$

We assume a linear relationship between g and the injected current I, which is defined as

$$g = \beta I, \tag{8}$$

where β is the gain factor. From Eqs. (7) and (8), the threshold current (I_{th}) of the two-section QD laser can be deduced as

$$I_{th} = \frac{1}{\beta L_g}\left[(\alpha+\varepsilon)L_a + \frac{1}{2}\ln\frac{1}{R^2}\right]. \tag{9}$$

From Eq. (8), we get

$$I_{\rm th} \propto (\alpha + \varepsilon), \tag{10}$$

$$\Delta I_{\rm th} \propto \Delta(\alpha + \varepsilon), \tag{11}$$

$$I_{\rm th} \propto L_{\rm a}. \tag{12}$$

As mentioned above, ε is proportional to the carrier extracting driven by the reverse voltage. At a given applied reverse voltage, carrier extracting first increases linearly with increasing light intensity and then achieves a stable value at a high intensity level, so is ε. On the other hand, it can also be imagined that with increasing reverse voltage, more carriers can be extracted out of the SA section, i.e., higher ε, which results in increasing $I_{\rm th}$ according to Eq. (9). Additionally, the loss coefficient α parabolically decreases with increasing light intensity[4], which originates from the saturation of the QD ground state population. So, the total loss coefficient is decided by the competition between α and ε with light intensity. As discussed above, ε is more difficult to saturate for a higher reverse voltage. It can be deduced that the decreasing rate of total loss $\Delta(\alpha+\varepsilon)$ is lowered with increasing reverse voltage. To further clarify, we define two parameters, P_1 and P_2. P_1 represents the intensity of spontaneous emission just before the lasing start, and it is almost the same for different SA lengths and reverse bias voltages. P_2 represents the critical light intensity at which the SA section converts from the transparent state to the non-transparent state. For a longer SA length, more input light is needed to maintain the carrier saturation of the ground states, i.e., higher P_2. For the same length of SA section, as shown in Fig. 2, both P_1 and P_2 are almost the same with different $V_{\rm a}$. So at a specific range of light intensity of $(P_2 - P_1)$, a higher reverse bias voltage can result in the narrowing of hysteresis width, as expressed by Eq. (11).

On the other hand, the loss coefficient α is proportional to the total density of QD states in the SA section. So, it can be inferred that $\alpha \propto L_{\rm a}$, and the changing rate of α versus light intensity gets slower with longer $L_{\rm a}$. The longer $L_{\rm a}$ is, the higher α is at the same light intensity, which increases $I_{\rm th}$ according to Eqs. (10) and (12). The larger difference between P_1 and P_2 with longer $L_{\rm a}$ results in an increasing difference between $\alpha(P_2)$ and $\alpha(P_1)$, and finally the broadening of the hysteresis loop. Similarly, if the stacked number of QD layers are added, the loss coefficient α is also expected to increase accordingly, which can explain the larger hysteresis width observed in our case.

Due to the slow changing rate of α with a long SA section, we can also deduce that the reverse bias voltage-induced changes of total loss coefficient are more significant than those of the short SA section, which results in larger changes in hysteresis width under different $V_{\rm a}$ with longer $L_{\rm a}$. Figure 5 shows that the reverse bias voltage induced changes in hysteresis width are larger for the sample with a longer SA, from which we can further prove our deduction.

4. Conclusion

In summary, we have fabricated two-section QD lasers with an integrated intracavity QD saturable absorber. In addition to achieving CW lasing operation at room temperature, we have also found the optical bistability when the SA section is under an appropriate bias condition. The hysteresis width is narrowed with increasing reverse bias voltage, and broadened with increasing length of SA. According to a modified threshold current modal, we find that the hysteresis width is determined by competition of the QD absorption and the electroabsorption, and can also be affected by the number of stacked QD layers. Our conclusions are expected to be helpful in the understanding and design of lasers with optical bistability.

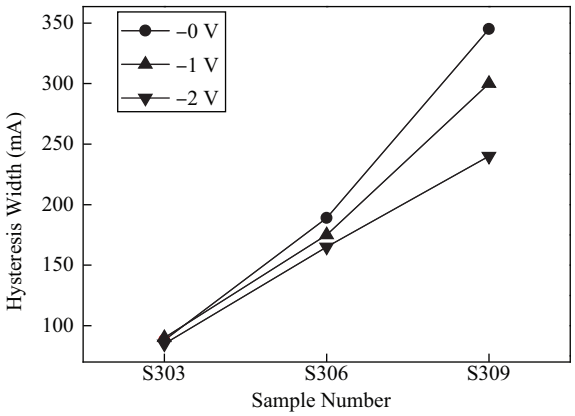

Fig. 5. Hysteresis width of three samples under different reverse bias voltages.

Acknowledgements

The authors would like to acknowledge Liang Ping and Hu Ying for their help with device fabrication.

References

[1] Rafailov E U, Cataluna M A, Wilcox K, et al. Compact ultrafast lasers based on quantum-dot structures. Proc SPIE, 2009, 7222: 72220I

[2] Malins D B, Gomez-Iglesias A, White S J, et al. Ultrafast electroabsorption dynamics in an InAs quantum dot saturable absorber at 1.3 μm. Appl Phys Lett, 2006, 89(17): 171111

[3] Qasaimeh O, Zhou W D, Philips J, et al. Bistability and self-pulsation in quantum-dot lasers with intracavity quantum-dot saturable absorbers. Appl Phys Lett, 1999, 74(12): 1654

[4] Huang X D, Stintz A, Li H, et al. Bistable operation of a two-section 1.3 μm InAs quantum dot laser-absorption saturation and the quantum confined stark effect. IEEE J Quantum Electron, 2001, 37(3): 414

[5] Shi L W, Chen Y H, Xu B, et al. Status and trends of short pulse generation using mode-locked lasers based on advanced quantum-dot active media. J Phys D, 2007, 40(18): R307

[6] Thompson M G, Rae A R, Xia M, et al. InGaAs quantum-dot mode-locked laser diodes. IEEE J Sel Topics Quantum Electron, 2009, 15(3): 661

[7] Thompson M G, Tan K, Marinelli C, et al. Transform-limited optical pulses from 18 GHz monolithic mode locked quantum dot lasers operating at 1.3 μm. Electron Lett, 2004, 40: 346

[8] Thompson M G, Rae A, Sellin R L, et al. Subpicosecond high-power mode locking using flared waveguide monolithic quantum-dot lasers. Appl Phys Lett, 2006, 88 (13): 133119